J|A|C|S
ARTICLES
Published on Web 12/27/2001

Synthesis, Structure, and Bonding of $BaTl_3$: An Unusual Competition between Cluster and Classical Bonding in the Thallium Layers

Dong-Kyun Seo and John D. Corbett*

Contribution from the Ames Laboratory—DOE[1] and Department of Chemistry, Iowa State University, Ames, Iowa 50011

Received July 16, 2001

Abstract: The new $BaTl_3$ compound has been synthesized and characterized by physical property measurements and electronic structure calculations. Its structure (*Cmcm*) is a new intermediate in the Ni_3Sn family ($P6_3/mmc$), and consists of thallium layers formed from two-center bond formation between the parallel chains of face-sharing octahedral clusters. The valence electron concentration (VEC) of the thallium layers is consistent with their two-dimensional nature, in comparison with those in other AX_3-type compounds with one- or three-dimensional anionic networks with the same building blocks and different VECs. The unique geometric features of the anionic thallium layers bring on an unusual competition between inter- and intracluster bonds. Detailed studies of the energetics of $BaTl_3$ reveal for the first time the important role of cation−anion interactions in the bonding competition in such an anionic substructure.

Introduction

Reduction of posttransition metals by alkali and alkaline-earth metals frequently leads to polar intermetallics that contain polyanions of these p-elements. Recent research efforts, especially on alkali-metal compounds, have revealed that the structures of such polar intermetallics are far more diverse than and beyond the grasp of Zintl concepts, classical valence rules that have long been a guide to understanding this class of compounds. A new paradigm has emerged and is still being refined, one that accommodates modern bonding concepts and recognizes competitive factors (beyond electronic effects) in structural stabilization, Madelung energy, and packing efficiency, for instance.[2] The scarcely explored alkaline-earth-metal−triel (or rare-earth-metal−triel) systems look particularly suitable for the study of these additional factors in detail because of their higher cation charges, lower cation populations, and strong covalency. In fact, our recently initiated explorations of alkaline-earth-metal−triel systems have already revealed notable examples that show the importance of cation effects in structure-type selection and the stabilization of unusual electron deficiencies in the anionic sublattices.[3,4] These new results urge more balanced views in the field of polar intermetallic chemistry in which electronic structures of anionic sublattices have heretofore been the main interest in consideration of chemical and electronic structure relationships.

Among the polar intermetallics with divalent/trivalent metal cations (A) and anions of the group 12−14 elements (X), certain compounds with the composition of AX_3 are particularly interesting because *both* atom size and electronic effects play important roles in structure selection. In their extremes, these exhibit the $AuCu_3$ ($Pm\bar{3}m$; Figure 1a) and Ni_3Sn ($P6_3/mmc$; Figure 1b,c) type structures; the former is a ccp packing of Kagome-type anionic layers of X atoms and the latter is a hcp packing of these.[5,6] The different patterns give rise to octahedra of X atoms in both structures, yet with different connectivities of the octahedra. In the $AuCu_3$ type, the octahedra share corners along all three directions, whereas in the Ni_3Sn type they share faces along the 6-fold axis to form chains that may or may not be connected through interchain (or intercluster) bonds perpendicular to the chain axis. Combinations of the two packing patterns result in intermediate structures, in which the cubic character in their structure types increases in the order of Ni_3Sn (*hhh*) < $BaPb_3$ (*hhc*) < β-$HfNi_3$ (*hhchc*) < $TiNi_3$ (*hchc*) = $PuGa_3$ (*hhcc*) < β-$HoAl_3$ (*hchcc*) < β-$PuAl_3$ (*hcc*) < $AuCu_3$ (*ccc*).[7−9] It has been established from the studies of RAl_3 (R = rare-earth element) that this structural series is related to the size of cations in such a way that smaller cations generate the $AuCu_3$-type structure whereas the Ni_3Sn-type structure occurs with larger cations.[7]

The electronic structure of the $AuCu_3$-type AX_3 compounds has been studied in detail with an aluminum representative sublattice to reveal that the optimum number of electrons is eight per Al_3.[9] However, assuming the validity of a rigid band

(1) This research was supported by the Office of the Basis Energy Sciences, Materials Science Division, U.S. Department of Energy. The Ames Laboratory is operated for the DOE by Iowa State University under Contract No. W-7405-Eng-82.
(2) Corbett, J. D. *Angew. Chem., Int. Ed.* **2000**, *39*, 682.
(3) Seo, D.-K.; Corbett, J. D. *J. Am. Chem. Soc.* **2000**, *122*, 9621.
(4) Seo, D.-K.; Corbett, J. D. *J. Am. Chem. Soc.* **2001**, *123*, 4512.
(5) Villars, P.; Calvert, L. D. *Pearson's Handbook of Crystallographic Data for Intermetallic Phases*, 2nd ed.; American Society of Metals: Metals Park, OH, 1991.
(6) O'Keeffe, M.; Hyde, B. G. *Crystal Structures—I. Patterns and Symmetry*; Mineralogical Society of America: Washington, DC, 1996; p 256.
(7) (a) Van Vucht, J. H. N.; Buschow, K. H. J. *J. Less-Common Met.* **1965**, *10*, 98. (b) Cirafici, S.; Franceschi, E. *J. Less-Common Met.* **1981**, *77*, 269.
(8) Xu, Z.; Guloy, A. M. *J. Am. Chem. Soc.* **1998**, *120*, 7349.
(9) Vajenine, G.; Hoffmann, R. *J. Am. Chem. Soc.* **1998**, *120*, 4200.

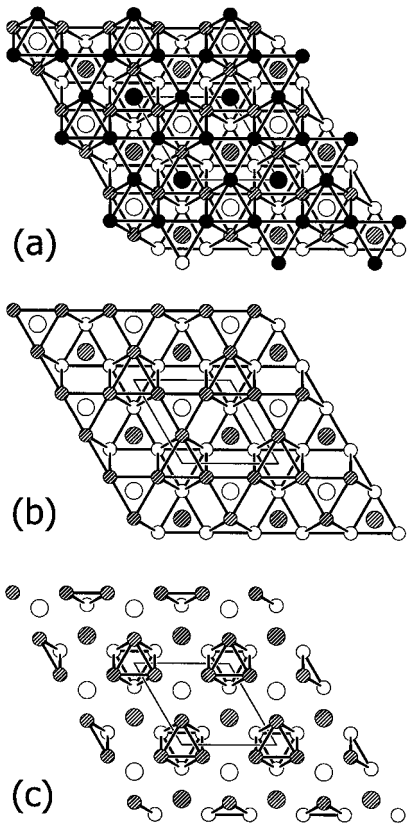

Figure 1. Projection views of (a) $AuCu_3$, (b) Ni_3Sn type I, and (c) Ni_3Sn type II structures normal to the stacked Kagome-type layers ((a) and (b) are adapted from ref 6). The atoms in *A*, *B*, and *C* layers of the stacking sequences are represented by open, shaded, and closed circles in the order of the height along the *c*-axis. The small circles indicate the atoms in the Kagome-like layers, and the larger ones correspond to the counter atoms.

approximation, the observed large variation of the formal valence electron concentration (VEC)—from 5 (for example, $AePd_3$; Ae = alkaline-earth element) to 14 (RTt_3; Tt = Si, Ge, Sn, Pb)—indicates a remarkable flexibility to the structure. The electron deficiency or excess is accommodated simply by changing overall anion−anion bond distances in the triangular rings in the Kagome nets, which are all equivalent in the cubic symmetry.[9]

On the other hand, the AX_3 compounds in the Ni_3Sn-type family, which have not been systematically studied before, seem to have another way to adjust their structures to their number of valence electrons. When these compounds have no more than nine valence electrons per X_3, the inter- and intrachain distances are almost the same in a three-dimensional anionic network, Figure 1b (our structure type I).[10] However, when the VEC per X_3 is 12 or higher, the anionic structure becomes one-dimensional, Figure 1c (structure type II), with much longer interchain distances. In these cases, the interchain bonds are broken and lone-pair formation accommodates the electron abundance, as in the superconductor $BaSn_3$.[11]

In the present work, we report the new compound $BaTl_3$ with 11 valence electrons per Tl_3, i.e., with an intermediate VEC. The electronic effects on its structural features must be important because the new structure exhibits two-dimensional layers of thallium atoms, making it a structural intermediate between the three- and one-dimensional anionic lattices. Detailed electronic and Madelung energy calculations reveal a surprising cation effect that has not been noted so far.

Experimental Section

Synthesis. According to the powder pattern, the title compound is obtained as a single phase (≥95% yield) following direct fusion of stoichiometric amounts of Ba (Alfa-Aesar, 99.9%) and Tl (Johnson Matthey, 99.998%) in welded tantalum containers[12] sealed in an evacuated silica jacket at 900 °C for 12 h followed by cooling at 10 °C/h to 500 °C and annealing at 500 °C for 7 weeks. The reaction was then quenched to room temperature in water. This procedure gives a brittle gray metallic-appearing product, and there is no indication of reaction of the sample with the Ta tube. The reaction was originally designed to synthesize the high-temperature form of $BaTl_3$, whose existence was reported in the literature in addition to a low-temperature phase, but both without crystallographic information.[13] However, the powder pattern from our high-temperature synthesis was no different from that obtained for the low-temperature product (annealed at 350 °C for 4 weeks), leading to the conclusion that $BaTl_3$ has the same structure in the entire temperature region before melting or decomposition.

The absence of hydrogen in the target compound was ensured by another set of syntheses with the Ta container under dynamic high vacuum with a trap cooled with liquid N_2 placed between the line and the outer silica tube.[14] First, to rule out the possible existence of hydrogen in the starting materials, Ba especially, 400−600 mg of barium metal was sealed in a Ta container, which was in turn placed in a fused silica tube connected to the vacuum system, heated at 900 °C for 12 h in the dynamic vacuum, and allowed to cool to room temperature radiatively. The barium exhibited a brighter luster after the treatment. The syntheses under dynamic vacuum with this purified barium metal were done first by direct fusion of the elements at 700 °C for 1 h, followed by cooling at 50 °C/h to 600 °C, then by cooling at 10 °C/h to 400 °C, and finally by cooling at 20 °C/h to room temperature. The X-ray powder pattern of the reaction product also revealed the $BaTl_3$ phase in ~80% yield, which proved that the $BaTl_3$ phase is not a hydride because tantalum metal at temperatures above 550 °C acts as a semipermeable membrane to hydrogen, but reacts with carbon and oxygen.

Structure Determination. A shiny, silvery block-shaped crystal ~0.11 × 0.09 × 0.13 mm was mounted in a glass capillary inside the glovebox. The crystal quality was first checked with Laue photographs, and then transferred to a Bruker SMART1000 CCD-equipped X-ray diffractometer for data collection, which took place at 23 °C with monochromated Mo Kα radiation. A total of 1027 frames was collected with the exposure time of 30 s/frame. The reflection intensities were integrated with the SAINT subprogram in the SMART software package[15] for the orthorhombic unit cell initially indicated from indexing 103 reflections. This process yielded a total of 1531 reflections, out of which 362 were independent and 266 had intensities greater than $2\sigma(I)$.

The XPREP subprogram in the SHELXTL software package[16] was used for the space group determination, in which systematic absences indicated *Cmcm*, *Cmc*2_1, and *Ama*2 as possible space groups. The centric space group *Cmcm*, which has the highest symmetry, allowed the most satisfactory refinement results in the later steps, although intensity statistics alone did not show a clear indication of a centrosymmetric space group ($\langle E^2 - 1 \rangle = 0.889$). All the atomic positions were located according to the Patterson method. Data were corrected for

(10) The structure types I and II are not distinguished by their crystallographic symmetries, and have neither been noted nor described in the literature. Our classification is solely based on their more obvious differences in structure and bonding.
(11) Fässler, T. F.; Kronseder, C. *Angew. Chem., Int. Ed. Engl.* **1997**, *36*, 2683.
(12) Corbett, J. D. *Inorg. Synth.* **1983**, *22*, 15.
(13) Bruzzone, G. *Ann. Chim.* **1966**, *56*, 1306.
(14) Leon-Escamilla, E. A.; Corbett, J. D. *J. Solid State Chem.* **2001**, *159*, 149.
(15) *SMART*; Bruker AXS, Inc.; Madison, WI, 1996.
(16) *SHELXTL*; Bruker AXS, Inc.; Madison, WI, 1997.

Table 1. Selected Data Collection and Refinement Parameters for $BaTl_3$

space group, Z	*Cmcm* (no. 63), 4
fw	750.44
lattice parmeters (Å, deg)[a]	$a = 7.024(1)$, $b = 13.899(2)$, $c = 5.201(1)$ Å
ρ_{calcd} (g cm^{-3})	5.911
μ (Mo Kα, cm^{-1})	622.5
R1, wR2[b]	0.060, 0.064

[a] Guinier powder pattern data; $\lambda = 1.540\,562$ Å. [b] $R1 = \sum||F_o| - |F_c||/\sum|F_o|$, $wR2 = [\sum w(|F_o|^2 - |F_c|^2)^2/\sum w(F_o^2)]^2$, where $w = 1/[\sigma^2(|F_o|^2)]$.

Table 2. Atomic Coordinates ($\times 10^4$ Å) and Isotropic Equivalent Displacement Parameters ($\times 10^3$ Å^2) for $BaTl_3$

		x	y	z	B_{eq}[a]
Tl(1)	*m*2*m*	0	1264(1)	2500	27(1)
Tl(2)	*m*	2401(1)	4317(1)	2500	26(1)
Ba	*m*2*m*	0	6914(1)	2500	21(1)

[a] B_{eq} is defined as one-third of the trace of the orthogonalized U_{ij} tensor.

Table 3. Selected Bond Distances (Å) and Bond Angles (deg) in $BaTl_3$

Tl(1)−Tl(2)[a]	3.265(1) × 2	Tl(2)−Tl(1)−Tl(2)[a]	67.99(4)
Tl(1)−Tl(2)	3.278(1) × 4	Tl(2)−T1(1)−Tl(2)	58.97(2)
Tl(1)−Ba[a]	3.626(1) × 2	Tl(2)−Tl(2)−Tl(2)[b]	107.69(4)
Tl(1)−Ba	3.630(1) × 2	Tl(1)−Tl(2)−Tl(1)[b]	104.98(3)
Tl(2)−Tl(2)	3.221(1) × 2	Tl(2)−Tl(2)−Tl(2)	90.0
Tl(2)−Tl(1)	3.265(1)	Tl(1)−Tl(2)−Tl(2)	123.84(2)
Tl(2)−Tl(1)	3.278(1) × 2		
Tl(2)−Tl(2)[a]	3.372(2)		
Tl(2)−Tl(2)[a]	3.652(2)		
Tl(2)−Ba	3.540(1) × 2		
Tl(2)−Ba[a]	3.806(1)		
Tl(2)−Ba[a]	3.984(2)		
Ba−Tl(2)	3.540(1) × 4		
Ba−Tl(1)[a]	3.626(1) × 2		
Ba−Tl(1)	3.630(1) × 2		
Ba−Tl(2)[a]	3.806(1) × 2		
Ba−Tl(2)[a]	3.984(2) × 2		

[a] Bond distances and angles within the planes at $z = 1/4$ or 3/4. [b] Bond angles between atoms zigzagging along the *c*-axis.

absorption by the XPREP subprogram initially and by the DIFABS program[17] after isotropic refinement.[18] The full-matrix least-squares refinement converged at $R(F) = 6.0\%$, $wR2 = 6.4\%$, and GOF = 1.04 for 15 variables and 362 independent reflections ($I > 0$). The largest residual peak and hole in the ΔF map were 3.7 and −3.6 e$^-$/Å^3, respectively. Some aspects of the data collection and refinement are listed in Table 1. Table 2 gives the atomic positional and isotropic equivalent displacement parameters, and Table 3 lists important interatomic distances and bond angles in the structure. More detailed crystallographic information as well as the anisotropic displacement parameters are available in the Supporting Information.

Properties. Electrical resistivities were measured at 35 MHz over 100−260 K by the electrodeless "Q" method with the aid of a Hewlett-Packard 4342A Q Meter.[19] For this purpose, 148.1 mg of a pure powdered sample with grain diameters between 150 and 250 μm was dispersed with chromatographic alumina and sealed under He in a Pyrex tube. Magnetic susceptibility measurements were carried out at 3 T over 8−300 K on a Quantum Design (MPMS) SQUID magnetometer. The powdered sample was held between the faces of two fused silica rods that were in turn fixed and sealed inside a silica tube. The data were corrected for the container and the standard diamagnetic core contributions ($\chi_{dia} = -134 \times 10^{-6}$ emu/mol).

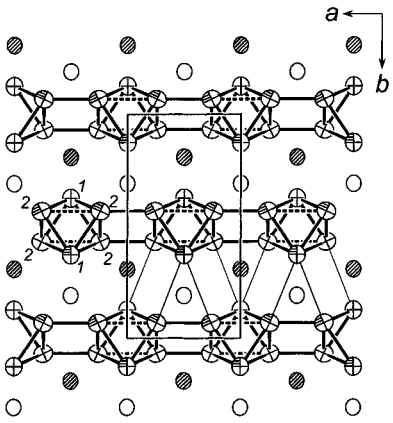

Figure 2. A [001] section of the orthorhombic unit cell of $BaTl_3$ down the short *c*-axis: 99% ellipsoids. All atoms lie in the same type of the planes at $z = 1/4$ (crossed thallium and open barium) or 3/4 (quarter-shaded thallium and shaded barium) in this projection. Thallium layers are formed by the condensation along the *a*-axis of the chains of face-sharing chains of octahedra that run along $\vec{c}$, and the layers are stacked along the *b*-axis with a translational vector of $(\vec{a} + \vec{b})/2$ owing to the *C*-centering. The thick lines indicate Tl−Tl bonds within 3.4 Å, and the thick broken lines represent longer intrachain Tl2−Tl2 bonds (3.65 Å). Some of the shortest interlayer thallium distances (4.57 Å) are marked by thin lines.

EHTB and Madelung Energy Calculations. All the extended Hückel tight binding (EHTB) band calculations were carried out using the CAESAR program.[20] A weighted H_{ij} formula was used for the extended Hückel calculations, and the following atomic orbital energies and exponents were employed for all the calculations (H_{ii} = orbital energy, ζ = Slater exponent): Tl 6s, $H_{ii} = -11.6$ eV, $\zeta = 2.3$; 6p, −5.8 eV, 1.6;[21] Ba 6s, −5.49 eV, 1.21; 6p, −3.56 eV, 1.21.[22] Madelung energies were calculated with the MAD program.[23]

Results and Discussion

Structure. $BaTl_3$ represents a new and remarkable structure type that bridges between the two extremes of the hexagonal Ni_3Sn-type structures (Figure 1b,c), one that has a three-dimensional anionic network and the other with isolated one-dimensional chains. In Figure 2, a [001] projection view of the $BaTl_3$ structure shows *two-dimensional* layers of thallium atoms (crossed and quarter-shaded ellipsoids) which are separated by barium atoms (open and shaded ellipsoids). All atoms in the structure lie at $z = 1/4$ (crossed thallium and open barium) or 3/4 (quarter-shaded thallium and shaded barium) in this projection. Like the X atoms in the Ni_3Sn-type AX_3 compounds, thallium atoms in $BaTl_3$ form nominally octahedral clusters which share opposed faces to generate chains normal to the figure (along $\vec{c}$). All the chains, equivalent by symmetry, are parallel. However, differently from either of the two extremes

(17) Walker, N.; Stuart, D. *Acta Crystallogr. A* **1983**, *39*, 158.
(18) The DIFABS-treated data resulted in a slightly better final structure for $BaTl_3$ than that without the treatment. For example, when only the SADABS program was used for the absorption correction, the esd values of the atom positions and bond distances were larger by the factor of 2, and the thermal ellipsoids of all the atoms were elongated along the *a* axis by a maximum U_{11}/U_{ii} ($i = 2$ or 3) of 1.3−1.7. The B_{eq}, R_1, and difference electron density map values also were slightly higher before the DIFABS treatment. This slight nuisance in the crystallographic data, not unusual in view of the magnitude of the absorption coefficient (622.5 cm^{-1}), may be because of poorer crystallinity of the sample, although some merohedral twinning is not completely excluded either. However, the bond distances do not have significant uncertainties to alter our discussions in the following sections.
(19) Zhao, J.-T.; Corbett, J. D. *Inorg. Chem.* **1995**, *34*, 378.
(20) Ren, J.; Liang, W.; Whangbo, M.-H. *CAESAR for Windows*; Prime-Color Software, Inc., North Carolina State University: Raleigh, NC, 1998.
(21) (a) Whitmire, K. H.; Ryan, R. R.; Wasserman, H. J.; Albright, T. A.; Kang, S. K. *J. Am. Chem. Soc.* **1986**, *108*, 6831. (b) Janiak, C.; Hoffmann, R. *J. Am. Chem. Soc.* **1990**, *112*, 5924.
(22) The H_{ii} values of Ba are from: Vela, A.; Gázquez, J. L. *J. Phys. Chem.* **1988**, *92*, 5688. The ζ values are obtained from the extrapolation of the ζ's of Ca and Sr reported in the following references, respectively: Zheng, C.; Hoffmann, R. *J. Am. Chem. Soc.* **1986**, *108*, 3078; Jaffé, H. H.; Hinze, J. *J. Chem. Phys.* **1963**, *67*, 1501.
(23) Smith, M.; Miller, G. J. *J. Solid State Chem.* **1998**, *140*, 226.

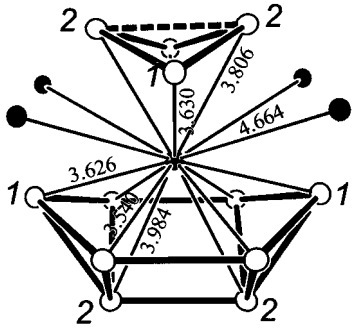

Figure 3. The C_{2v} environment around Ba in $BaTl_3$ in an off-[001] view. The thallium atoms are open ellipsoids, and the barium atoms are closed ellipsoids. The thallium clusters above and below the barium atom are parts of the neighboring layers.

of the Ni_3Sn-type structures (types I and II), the clusters in the neighboring chains in $BaTl_3$ are joined directly together along *one and only one* direction (*a* in this case) to form layers of chains perpendicular to the *b*-axis. The shortest interlayer thallium distance is 4.565 Å (thin lines) between Tl1 and Tl2 in adjacent layers.

The connection of the chains via interchain (or intercluster) exo bonds is rather unusual. While in many other cluster compounds, the classical exo bonds are oriented ~180° away from the center of the clusters, the exo bonds in $BaTl_3$ are parallel to one of the intracluster bonds (dashed lines in Figure 2), and the two sets of bonds—the Tl2−Tl2 bonds in octahedral clusters (intracluster bond) and the Tl2−Tl2 bonds between the clusters (intercluster bond; solid lines in Figure 2)—*compete against each other directly*. This competition is reflected in their bond distances that are longer than the others, 3.65 and 3.37 Å, respectively, whereas other thallium bond distances within the octahedral clusters range from 3.22 to 3.28 Å. An important conclusion is drawn from detailed bond length comparisons in a later section.

Meanwhile, the lowered symmetry caused by layer formation results in a strongly distorted environment around barium atoms, Figure 3. Each barium atom lies directly above the center of a boat-shaped pocket of six atoms from two clusters in one thallium layer. A side of an octahedral chain in the neighboring layer is located opposite this boat, and the Tl1 and barium atoms zigzag along the *c*-axis. Without the layer-forming distortion, a trigonal prism of thallium atoms would be the environment of each barium atom. The distances between barium and eight nearby thallium atoms in the $BaTl_3$ structure range from 3.54 to 3.63 Å. The barium atoms form puckered Kagome nets of equivalent isosceles triangles between the thallium layers, and the shortest Ba−Ba distance is 4.66 Å.

Bonding Scheme. The electronic band structure was calculated for the complete structure of $BaTl_3$ with the extended Hückel tight binding (EHTB) method. The total and projected densities of states (DOS) and the crystal orbital overlap populations (COOP) from the calculations are plotted in Figure 4, in which the 11 valence electrons per formula unit fill the bands up to a Fermi energy of −4.4 eV. The band structure does not exhibit a band gap, indicating a metallic property. The optimum number of valence electrons to fill all the bonding states is close to 10.5 per formula. The Fermi level lies in a weakly Tl−Tl antibonding region, and hence the compound is slightly electron rich. Thallium 6s bands are located far below

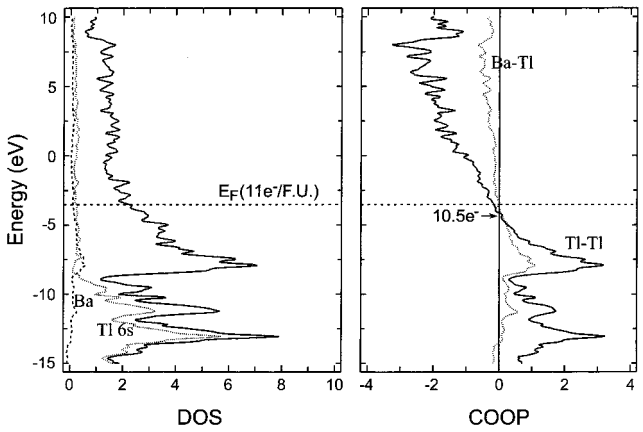

Figure 4. (a) DOS and (b) COOP plots calculated for $BaTl_3$. In (a), the solid, dashed, and dotted lines refer to total DOS, the PDOS of Ba, and the PDOS of Tl 6s, respectively. The Fermi level (E_F) is shown as a horizontal dashed line. In (b), the solid and dotted lines represent COOP for all Tl−Tl bonds within 3.7 Å and for all Ba−Tl contacts within 4.0 Å, respectively. The arrow indicates the upper energy level that would be occupied by 10.5 valence electrons.

the Fermi level, while the 6p orbitals dominate near the Fermi level. The contributions of barium below the Fermi level is small, and the calculated gross valence electron populations on Ba is 0.43 electrons per atom (1.57+). The corresponding values for Tl1 and Tl2 are 3.59 (0.59−) and 3.49 (0.49−), respectively.

The rather complicated catenation pattern within the thallium layers in $BaTl_3$ requires a lengthy analysis for a complete appreciation, but we will limit our discussions to a simplistic picture of the bonding scheme. In their work on $BaSn_3$ (14 valence electrons per Sn_3) with the Ni_3Sn type II structure (Figure 1c), Fässler et al.[11] argued that the Sn_3^{2-} triangles in *ab*-plane are isoelectronic with aromatic 2π-electron cyclopropanyl cations ($C_3R_3^+$) (**1**), and that the isolated chains of face-

Scheme 1

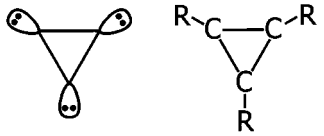

1

sharing octahedra may be viewed as stacked antiprismatic triangular units, with strong interactions between the component π systems along the chains. Their LMTO and EHTB calculations showed that the three lone pair orbitals that point away from the center of each triangle are all filled, which is in agreement with their arguments. It is reasonable to assume that those lone pair orbitals are also all filled even in the isostructural RAl_3 systems, although these compounds are two electrons poorer than the $BaSn_3$, because the face-sharing octahedral chains are still isolated in their structures. The π system is more likely to be empty of electrons here.

Further losses of electrons will remove electrons from the lone pairs and should therefore cause condensation of the cluster chains in the directions perpendicular to the chains via bond formation between the former lone pair orbitals. Experimentally, a complete condensation and the consequent three-dimensional network occur with three or four fewer electrons (nine or eight valence electrons per X_3), as found for the Ni_3Sn type I structure. Although not shown here for the integrity of the article, our

electronic structure analysis on an idealized three-dimensional aluminum network of the structure type I revealed that the optimum number of valence electrons is eight per X_3, and that this results both from a unique resonance bonding within the p-metal Kagome net and from multicenter bonds through σ and π orbitals along the *c*-axis.[25] Any extra π electrons in the Kagome net (or equally, the π electrons in the triangles) will fall in the antibonding region of the multiple bonds. Meanwhile, the optimum number of electrons per X_3 for the Ni_3Sn type II structure would be 12 (three skeletal bonds and three lone pairs per triangle), when the lone pairs are stabilized by the cations.[26]

Partial condensation of the octahedral chains as found in the $BaTl_3$ structure would require 10 valence electrons per X_3. This is because two of the three lone pair orbitals of a thallium triangle that lie nearly along the *a*-axis have to lose one electron each to form a classical bond with an orbital of the same type in the neighboring chain. This simple electron-counting scheme is well in agreement with our band calculation results in Figure 4.

Competition between Intra- and Intercluster Bonds.[27] One of the most interesting features of the $BaTl_3$ structure is the *straight* −Tl2−Tl2−Tl2− chains formed by the alternation of the relatively long intra- and intercluster bonds. In fact, the situation reminds us of the Peierls electronic instability that is inherent in one-dimensional systems with partially filled bands. However, it is not clear whether a Peierls instability is really responsible for this bond alternation. First, the orbital interactions may not be strong enough to drive the distortion because the intra- and intercluster bonds along the −Tl2−Tl2−Tl2− chains are already longer than the other bonds. Because of the corelike nature of the 6s orbitals of thallium atoms, the intra- and intercluster bonds in the linear −Tl2−Tl2−Tl2− chains have to compromise with only one p_σ orbital per site, and hence these are not effective. Second, the −Tl2−Tl2−Tl2− chains are not isolated but interact very strongly with each other and also with covalently bonded neighboring Tl1 atoms in the chain, adding a considerable elastic energy to the lattice. Furthermore, the electrostatic and covalent interactions with the adjacent barium atoms may not be ignored.

To elucidate the origin of the distortion, several different types of energies were calculated as the ratio of the intra- and intercluster bond distances (d_{intra}/d_{inter}) was varied. All the other Tl−Tl bond distances as well as the fractional coordinates of barium atoms were fixed at their experimental values. The total energy of a given structure was calculated by the summation of the electronic and Madelung energies: the former were obtained from the EHTB calculations, and the latter were calculated with the effective charges from the EHTB results and the Madelung energy calculation program MAD.[23] Figure 5 summarizes the results. The total energy curve for the $BaTl_3$ (filled circles) shows a minimum at d_{intra}/d_{inter} of ∼1.08, which is in good agreement with the experimental value, 1.083.[28] Without the barium atoms in the lattice (open circles), the maximum electronic energy occurs for an intracluster bond that is still longer than the intercluster bond, but much less

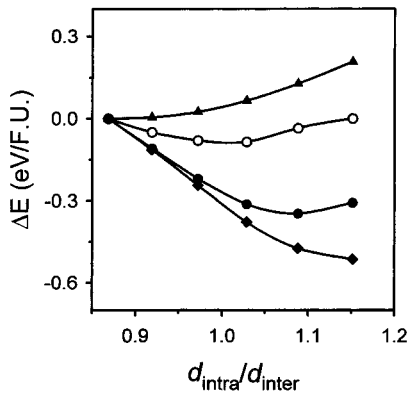

Figure 5. Calculated energy values as functions of the ratio of the intra- and intercluster bond (d_{intra}/d_{inter}) distances (see text). The filled triangles and open circles (top) are the total electronic energies calculated with and without the barium atoms. The calculated Madelung energies of the complete structure (with barium atoms) are plotted with the filled diamonds (bottom). The filled circles mark the total energies of the complete structure obtained from the sum of the electronic energies (filled triangles) and the Madelung energies (filled diamonds).

lengthened ($d_{intra}/d_{inter} \sim 1.01$). Therefore, it is clear that the covalent bonding in the thallium sublattice is not enough to explain the 1.08 ratio. A rather dramatic effect of barium can be seen for the separate electronic and Madelung energy results for the complete structures with the barium atoms included in the lattice (filled triangles and diamonds, respectively). The covalent energy alone favors a shorter intracluster bond ($d_{intra}/d_{inter} < 1$), which is the opposite of the experimental observation. However, this effect is completely overshadowed by the very strong preference of the Madelung energy for a shorter intercluster bond ($d_{intra}/d_{inter} > 1$), and hence the optimum structure has a shorter intercluster bond of the compound when the two energy terms are added.

The reason the electronic energy favors a shorter intracluster (and a longer intercluster) bond can be understood when the orbital interactions between Ba and Tl2 are considered. As the d_{intra}/d_{inter} ratio decreases (the intercluster bond lengthens), the orbital interactions between the cluster chains decrease as well, and the intercluster bonds along $\vec{a}$ will presumably break in the extreme. The lone-pair-like orbitals that would be liberated by a loosening of the intercluster bonds will now interact more efficiently with the valence orbitals of the neighboring barium atoms which are higher in energy, and hence the electronic energy will become lower. This may be possible because the intra- and intercluster bond distances are already longer, and hence the orbital interactions in these bonds are weak enough for the Ba−Tl orbital interactions to be comparable with them in magnitude. The effective charge versus d_{intra}/d_{inter} curves in Figure 6 illustrate indirectly how the Ba−Tl orbital interactions are affected as the d_{intra}/d_{inter} ratio changes. The effective charges on Ba and Tl2 become smaller as the ratio decreases (open and filled circles, respectively), while Tl1, which does not participate in the intercluster bonding (see Figure 2), shows no significant change in its effective charge (filled diamonds). The decrease in the effective charges results from a larger charge back-transfer

(24) Kauzlarich, S. M., Ed. *Chemistry, Structure and Bonding in Zintl Phases and Ions*; VCH: New York, 1996.
(25) Seo, D.-K.; Corbett, J. D. Unpublished results.
(26) Seo, D. K.; Corbett, J. D. *Science* **2001**, *291*, 841.
(27) A related, but different, competition has been reported between classical tetrahedral clusters of germanium or tin. See: Zürcher, F.; Nesper, R. *Angew. Chem., Int. Ed.* **1998**, *37*, 3314.
(28) This impressive result should be accepted with some caution. In our calculations, the electron densities were determined within the EH approximation, and were approximated as Mulliken point charges at nuclear positions for the Madelung energy calculations. The covalent bond energies depend on the atomic orbital parameters which were preselected. For example, when a more contracted Tl 6s orbital was used in the calculations, the energy minimum shifted to a larger d_{intra}/d_{inter} ratio.

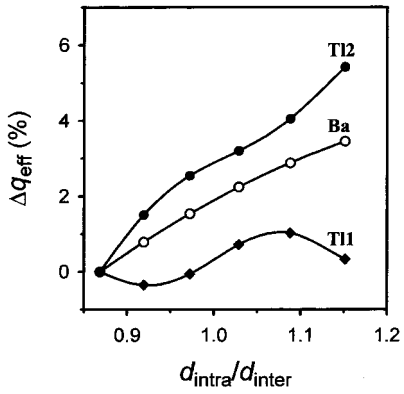

Figure 6. Changes in the calculated effective charges as functions of the ratio of the intra- and intercluster bond (d_{intra}/d_{inter}) distances (see text). The open circles, filled diamonds, and filled circles indicate the calculated effective charges of Ba, Tl1, and Tl2.

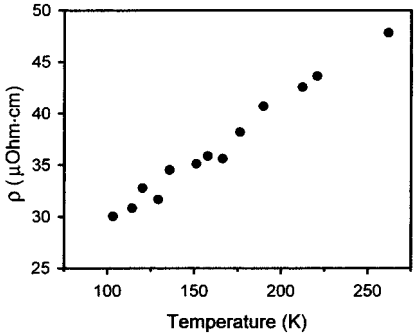

Figure 7. Temperature-dependent electrical resistivity of $BaTl_3$. Two sets of data are combined, one upon cooling and the other upon heating. No sign of hysteresis was observed.

from Tl2 anion to Ba cation, i.e., larger Ba−Tl2 orbital interactions (covalency).

The large changes in the effective charges of Ba and Tl2 also account for the behavior of the Madelung energy contribution in Figure 5. Simply, the higher the effective charges, the larger is the Madelung energy, i.e., with less charge back-transfer. Although the Ba−Tl distances were not optimized in the simulated structures, it was found from another set of calculations that the Madelung energy behavior is not because of the changes in the Ba−Tl distances, but really because of the drastic changes in the effective charges and cation−anion orbital interactions. That is, when Madelung energies were calculated with the same fixed charges for all the different structural variations, the calculated values slightly decreased as the d_{intra}/d_{inter} ratio increased, which disfavors a shorter intercluster bond.

Physical Properties. Figure 7 shows that the measured specific resistivities of $BaTl_3$ increase linearly from about 30 to 49 $\mu\Omega$·cm (0.22% K^{-1}) over the range of 100−260 K. The linear increase indicates that $BaTl_3$ is a normal metal in the temperature range of the measurement. This is in agreement with the prediction from our band calculation results. This metallicity of $BaTl_3$ can also be seen clearly in the Pauli paramagnetic behavior of the compound, measured over the range of 5−300 K, Figure 8.

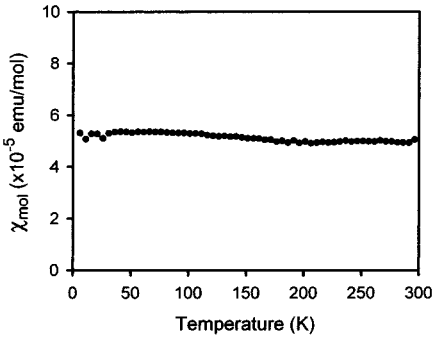

Figure 8. Molar magnetic susceptibility of $BaTl_3$ measured on heating at 3 T. The data indicate a Pauli paramagnetic compound.

Concluding Remarks

Over the decades, polar intermetallic chemistry has brought us many surprises that range from structural to electronic diversities. Violations of the Zintl rule seem to be fairly common especially among the triels,[2,24] and it is now our consensus that for such polar intermetallic compounds it is hard to generalize their structure−property relationships, if any. The origin of this troublesome nature in these polar intermetallics can be found in the weaker bonds between the p-elements near the Zintl boundary (between triels and tetrels). The covalent bonds in the frameworks made of these elements appear to be too weak to control or dominate the overall structural stabilities, and hence other energy terms, such as those from cation−anion interactions, can play important roles in the stabilization of the structures that apparently violate the Zintl rule.[29] This viewpoint, which balances the traditional electronic-factor-oriented views, has been explored and emphasized in our two recent papers.[3,4] Continuing this theme, our present work on the $BaTl_3$ now illustrates how important the cation−anion interactions can be in some polar intermetallics, well beyond our imagination.

Acknowledgment. D.-K.S. is grateful to Prof. G. J. Miller for the use of his MAD program.

Supporting Information Available: Tables of additional crystallographic data and anisotropic displacement parameters. (PDF) This material is available free of charge via the Internet at http://pubs.acs.org.

JA011728Y

(29) From another perspective, there is also a diminished electron affinity for the anion-forming elements, and a general disappearance of significant band gaps.